Advection of Momentum and Buoyancy in a Coastal Frontal Zone

J. O. BLANTON,* L.-Y. OEY,** J. AMFT* AND T. N. LEE@

*Skidaway Institute of Oceanography, Savannah, Georgia
**Department of Oceanography, Old Dominion University, Norfolk, Virginia
@Rosenstiel School of Marine and Atmospheric Science, University of Miami, Miami, Florida

(Manuscript received 4 June 1987, in final form 16 July 1988)

ABSTRACT

We report a study of a coastal frontal zone off the southeastern United States based on a field experiment and numerical modeling. The study was conducted in the spring of 1985 during weak to moderate wind stress and strong input of buoyancy from solar radiation and river discharge. The study confirms that the structure and slope of the frontal zone depends on a combination of wind stress and cross-shelf advection of buoyancy.

A cross-shore/depth two-dimensional (x, y), time-dependent numerical model illustrated the response of the frontal zone to the local wind stress regimes. A comparison of model results with field data showed that the model successfully predicted onsets of stratification and mixing. When alongshore wind stress was negative (southward), isopycnals in the frontal zone steepened due to a combination of horizontal advection and vertical convection. When stress was positive (northward), the offshore advection of low density water flattened the isopycnals and potential energy decreased, demonstrating that horizontal advection terms are important in the equation of conservation of buoyancy. The model predicts the offshore advection of lenses of less dense water during upwelling-favorable wind stress. These lenses are of the order of 20 km in cross-shelf scale and represent an efficient mechanism to export nearshore water. The lenses consist of a mixture of low-salinity coastal water and continental shelf water originating further offshore and advected onshore along the bottom.

The mean flow inside the frontal zone opposed the mean alongshore wind stress. Part of the alongshore flow was in geostrophy with the cross-shore pressure gradient; the other part was due to an alongshore pressure gradient force (kinematic) of about 1×10^{-6} m s^{-2} (equivalent sea surface slope = 1×10^{-7}), which was trapped along the coast with an offshore width scale of O(10 km). It is likely that the alongshore extent of this pressure gradient was governed by the scale at which freshwater is injected to the continental shelf, i.e., 20–30 km. The pressure gradient force immediately outside of the frontal zone was about -5×10^{-7} m s^{-2} in the direction of the mean alongshore wind stress. It is hypothesized that, as a result of wind setup and freshwater influx, the northward pressure gradient forced over outer shelf/slope by the Gulf Stream decreases in magnitude onshore, and can even change sign across a nearshore frontal zone of O(10 km). The implied flow field near the frontal zone is therefore highly three-dimensional with $|\partial v/\partial y| \approx |\partial u/\partial x|$, where ($u$, v) are velocities in the cross-shore (x) and alongshore (y) directions, respectively.

1. Introduction

Low density water is found along the coast of many continental shelves due to the discharge of rivers. This forms an offshore pressure gradient that requires transport to the right (Northern Hemisphere) of the low density water to balance the Coriolis force with the pressure gradient. This is the reason one often finds river plumes bent equatorward and a tendency for riverborne sediments to be transported equatorward.

This tendency is often masked by fluctuations in wind stress which can easily reverse the flow in shallow water against any alongshore pressure gradient. In studies of circulation in a coastal frontal zone off the Georgia coast (Blanton 1981, 1986), the aspect ratio of the frontal zone (slope of the isopycnals) and the sign of alongshelf currents depended upon the alongshelf direction of wind stress. Studies in the mid-Atlantic Bight (Beardsley and Winant 1979; Hopkins and Swoboda 1986) confirm that information on alongshelf winds and alongshelf pressure gradients, is required to understand observed fluctuations of currents in frontal zones in shallow water adjacent to coastlines.

Understanding of currents in the frontal zone off the southeastern United States has been hampered by the lack of time series data in water shallower than 15 m. Starting in 1985, we acquired current meter data along the 8-m and 15-m isobaths (Fig. 1). The shallow water moorings were deployed well inside of the band of low salinity water stretching for 400 km along the coast (Blanton 1981; Blanton and Atkinson 1983). Here, we report findings from these shallow water observations of currents and compare them with observations farther offshore. The differences offer some opportunity to understand the role of alongshore pressure gradients induced by low density water trapped along the coast. Any improved understanding should have some ge-

Corresponding author address: Dr. J. O. Blanton, Skidaway Institute of Oceanography, P.O. Box 13687, Savannah, GA 31416.

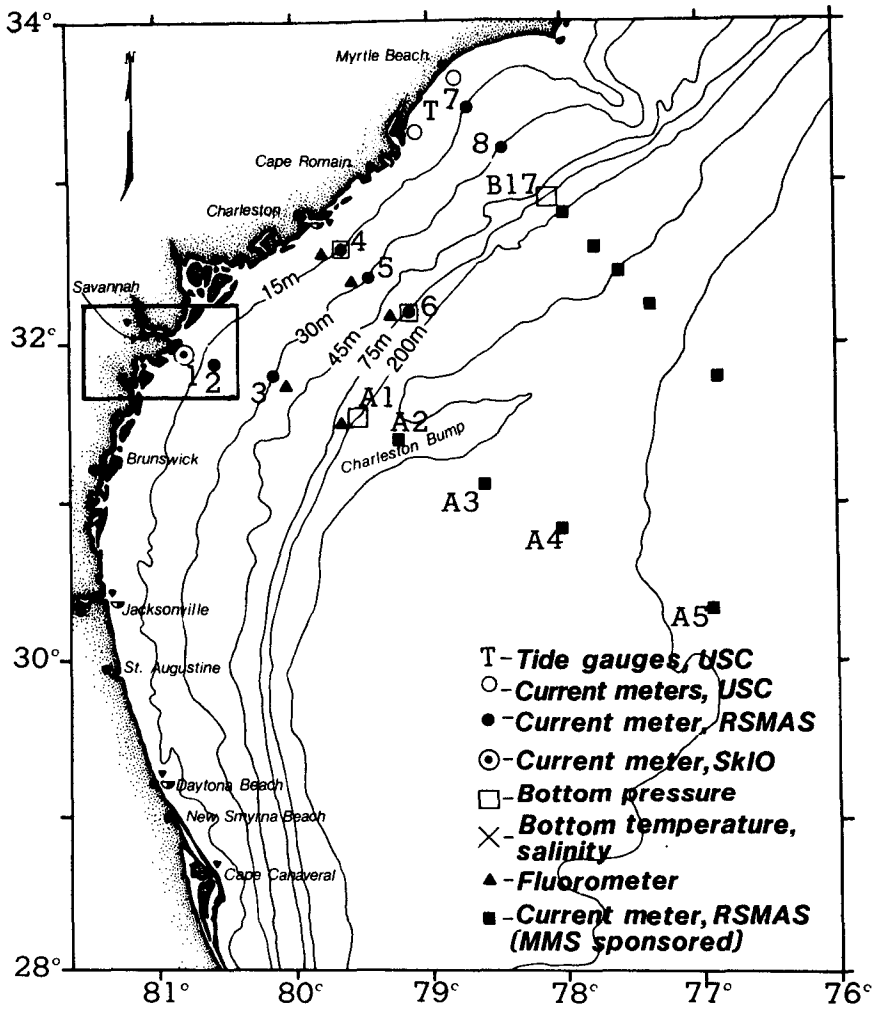

FIG. 1. Location map of the large scale arrays. The smaller-scale inner shelf array reported in this paper (Fig. 2) was located in the boxed area at Savannah, Georgia. (USC: University of South Carolina; RSMAS: Rosenstiel School of Marine and Atmospheric Sciences, University of Miami; SkIO: Skidaway Institute of Oceanography; MMS: Mineral Management Service).

neric value toward understanding circulation on other continental shelves.

2. Data

In the spring of 1985, a study of circulation was conducted to examine processes that remove accumulations of low density water from the coast off the southeastern United States. For this study we moored a set of current meters in the coastal frontal zone along with instruments which measured temperature, subsurface pressure, and conductivity (Fig. 2). The recording instruments were in place from late February to late June 1985 (Table 1).

The data from these instruments were edited and smoothed with a 3- and 40-h low-pass filter. The difference in the variances between the 3- and 40-h low-pass data reflect the predominant influence of tidal flow (Table 2). That is, most of the variance in ocean currents and other parameters occurred at semidiurnal frequencies. This report considers currents, temperature and salinity fluctuations at subtidal frequencies only, as reflected in the 40-h low-pass data. All vectors for wind stress and currents were placed in a coordinate system rotated −45 deg from east, so that the rotated x/y axes point southeastward/northeastward, respectively.

A series of seven hydrographic cruises was conducted in the study area. These data are used to describe the density structure in the frontal zone during April, about the middle of the study period. A moored conductivity cable at Savannah Navigational Light Tower (Station T, Fig. 2) provided additional data on density structure from April through June.

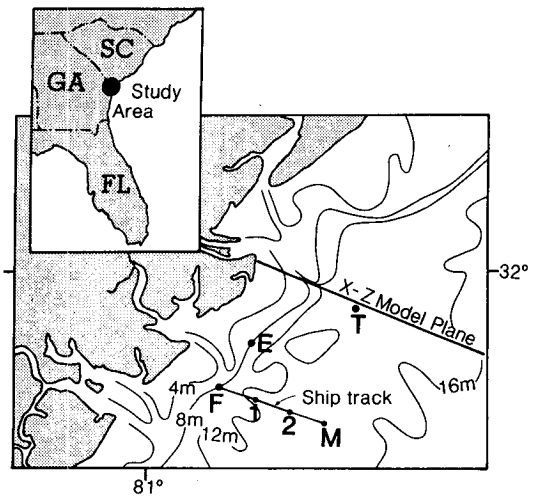

FIG. 2. Locations of moored instruments listed in Table 1. Wind stress and barometric pressure were measured at Station T. The F, 1, 2 and M represent hydrographic stations that were repeated seven times during the study.

3. Frontal zone during April 1985

During spring 1985, discharge of freshwater along the coast from South Carolina to Florida was one of the lowest in 20 years (see Blanton and Atkinson 1983, for description of seasonal fluctuations in river discharge). Nevertheless, there was a band of low density water inside of the 15-m isobath in the study area (Fig. 3).

Vertical density gradients ranged between 0 and 0.3 σ_t m^{-1}; horizontal gradients ranged between 0 and 0.2 σ_t km^{-1} (Fig. 3). These values were within the ranges observed previously (Blanton 1981). Zones of low sigma-t occasionally occurred near the surface in northern sections signifying the presence of local plumes of water from the Savannah River. These plumes were too near the surface to affect observations from our moored sensors.

4. Statistics of fluctuations

The average wind stress was northeastward with brief interrupted periods of stress to the southwest (Fig. 4). The strongest events in the record exerted southwestward stress during three episodes between 29 April and 9 May. The currents at Station T (Fig. 4) were predominantly northward and had a high visual correlation with wind stress.

The currents along the 8-m isobath appeared to respond more efficiently than currents further offshore to episodes of southward wind stress. During a period of calm winds between 7 and 24 April, there was strong southward flow at stations E and F but the southward flow at Station T was relatively weak.

A matrix of cross-spectra was computed for wind stress and for all current meters. A common period of 25 March to 1 June was chosen for analysis. An example of variance conserving spectra (Fig. 5) illustrates three peaks that were common to all records. The peak of the lowest frequency was centered about a period of

TABLE 1. Deployment dates and summary of instrument models and specifications used to measure various parameters during SPREX.

Station*	Deployment dates (mo/day 1985)	Parameter	Sensor	Range	Accuracy
T	2/18–6/20	Wind	Meteorology Research, Inc. 1074-2 wind sensor, speed: fast aluminum cups direction: damped aluminum vane	0–55 m s^{-1} 360°	±0.5 m s^{-1} ±4°
T	2/18–6/20	Barometric pressure	WeatherMeasure B242 analog barometer with multicell aneroid sensor	950–1050 mb	±1 mb
T_7, T_{12} E_6, F_6	2/18–6/1 3/25–6/20	Current	General Oceanics 6011 Mark II Niskin winged current meter speed: force-balance tilt sensor direction: three-axis flux gate compass	0–225 cm s^{-1} 360°	±1 cm s^{-1} ±2°
E_4	3/25–6/20	Current	InterOcean Systems, Inc. S4 current meter speed: electromagnetic, 2-axis sensor direction: flux gate magnetometer	0–350 cm s^{-1} 360°	±1 cm s^{-1} ±2°
T_{14}	4/16–6/20	Sub-surface pressure	Paroscientific digi-quartz pressure transducer (with Sea Data 642 logger)	0–60 m	0.9 cm
T_2, T_4, T_6, T_8, T_{11}, T_{14}	4/16–6/20	Water temperature	YSI 44030 precision thermistor (with Sea Data 642 Logger)	−5–+35°C	± −0.15°C
T_4, T_{11}, T_{14}	4/16–6/20	Conductivity	Sea-Bird Electronics SBE-4 conductivity meter (with Sea Data 642 logger)	0–70 mmho cm^{-1}	±0.01 mmho cm^{-1}

* Subscript denotes depth below sea surface in meters.

TABLE 2. Ranges, means and variances for parameters measured during SPREX. All parameters with x- and y-components have been rotated −45 deg. Series with a length of 66 days begin 27 March 1985 and series with a length of 46 days begin 16 April 1985; both end 1 June 1985.

Parameter	Min	Max	Mean	Variance (units)^2	Length (days)
		(a) 3-hour low-pass data			
Wind stress x-comp (dyn cm^{-2})	−3.45	4.87	−0.05	0.69	66
Wind stress y-comp (dyn cm^{-2})	−5.29	3.92	0.18	1.50	66
Barometric pressure (mb)	1000.1	1028.0	1015.4	20.96	66
T_7 current x-comp (cm s^{-1})	−51.56	38.21	−2.05	479.61	66
T_7 current y-comp (cm s^{-1})	−33.69	44.94	2.98	155.00	66
T_{12} current x-comp (cm s^{-1})	−38.11	34.96	−3.64	257.28	66
T_{12} current y-comp (cm s^{-1})	−29.59	26.22	1.23	76.91	66
E_6 current x-comp (cm s^{-1})	−29.83	35.11	−0.71	177.76	66
E_6 current y-comp (cm s^{-1})	−45.95	24.06	−0.78	86.50	66
F_6 current x-comp (cm s^{-1})	−35.75	35.64	−0.40	219.02	66
F_6 current y-comp (cm s^{-1})	−67.44	29.06	−2.86	176.00	66
E_4 current x-comp (cm s^{-1})	−36.15	40.06	0.89	245.69	66
E_4 current y-comp (cm s^{-1})	−34.31	30.78	−0.90	101.17	66
T_{14} sub-surface pressure (mb)	1237.2	1557.7	1391.0	4580.9	46
T_4 water temperature (°C)	17.19	25.34	21.75	4.51	46
T_{14} water temperature (°C)	17.29	24.64	21.49	4.37	46
T_4 salinity (ppt)	32.91	34.54	33.75	0.11	46
T_{14} salinity (ppt)	33.19	34.64	33.94	0.05	46
T_4 sigma-t	22.17	25.21	23.57	0.51	46
T_{14} sigma-t	22.76	25.25	23.79	0.38	46
		(b) 40-hour low-pass data			
Wind stress x-comp (dyn cm^{-2})	−2.39	3.20	−0.05	0.48	66
Wind stress y-comp (dyn cm^{-2})	−4.23	2.23	0.19	1.14	66
Barometric pressure (mb)	1000.6	1028.1	1015.47	20.41	66
T_7 current x-comp (cm s^{-1})	−10.82	6.97	−2.18	11.70	66
T_7 current y-comp (cm s^{-1})	−17.38	20.08	3.08	50.69	66
T_{12} current x-comp (cm s^{-1})	−12.72	7.34	−3.65	11.76	66
T_{12} current y-comp (cm s^{-1})	−13.35	11.65	1.18	22.85	66
E_6 current x-comp (cm s^{-1})	−7.95	6.32	−0.70	8.14	66
E_6 current y-comp (cm s^{-1})	−19.17	8.40	−0.79	20.84	66
F_6 current x-comp (cm s^{-1})	−8.60	4.92	−0.37	6.98	66
F_6 current y-comp (cm s^{-1})	−39.56	11.30	−2.85	61.76	66
E_4 current x-comp (cm s^{-1})	−5.67	5.29	0.93	6.02	66
E_4 current y-comp (cm s^{-1})	−20.13	10.66	−0.88	29.90	66
T_{14} sub-surface pressure (mb)	1374.8	1414.4	1390.9	93.69	46
T_4 water temperature (°C)	17.20	24.86	21.75	4.50	46
T_{14} water temperature (°C)	17.24	24.55	21.49	4.41	46
T_4 salinity (ppt)	33.26	34.31	33.75	0.08	46
T_{14} salinity (ppt)	33.36	34.60	33.95	0.05	46
T_4 sigma-t	22.49	25.19	23.57	0.49	46
T_{14} sigma-t	22.92	25.22	23.80	0.38	46

15 days. The largest peaks were centered on periods between 3.5 to 6 days, hereafter called the 5-day band. A prominent secondary peak also occurred at periods less than 2 days. These peaks were in response to fluctuating wind stress due to the passage of weather fronts.

We have summarized the variances at subtidal frequencies represented by these peaks (Table 3). The variances were greatest at the upper current meter at Station T and at Station F. The variances at the other three meters were smaller by a factor of 2. The stability of the elliptical properties of the vector fluctuations were generally above 0.5, indicating the rotary characteristics of the vector were statistically repeatable. We concentrate on the rotary characteristics of wind, surface current and bottom current in the energetic 5-day band (Fig. 6). The wind vector rotated clockwise (anticyclonically). The current vector near the surface at Station E rotated cyclonically. The current vectors near bottom at E, and F oscillated more rectilinearly than those closer to the surface.

The coherence-squared and phase lag between alongshore components of wind and currents in the 5-day band (Table 4) were greater than 0.7 and less than 10 hours. Greatest coherence and smallest lag with the wind occurred along the 8-meter isobath. In fact, all current meters and the wind in the 5-day band are

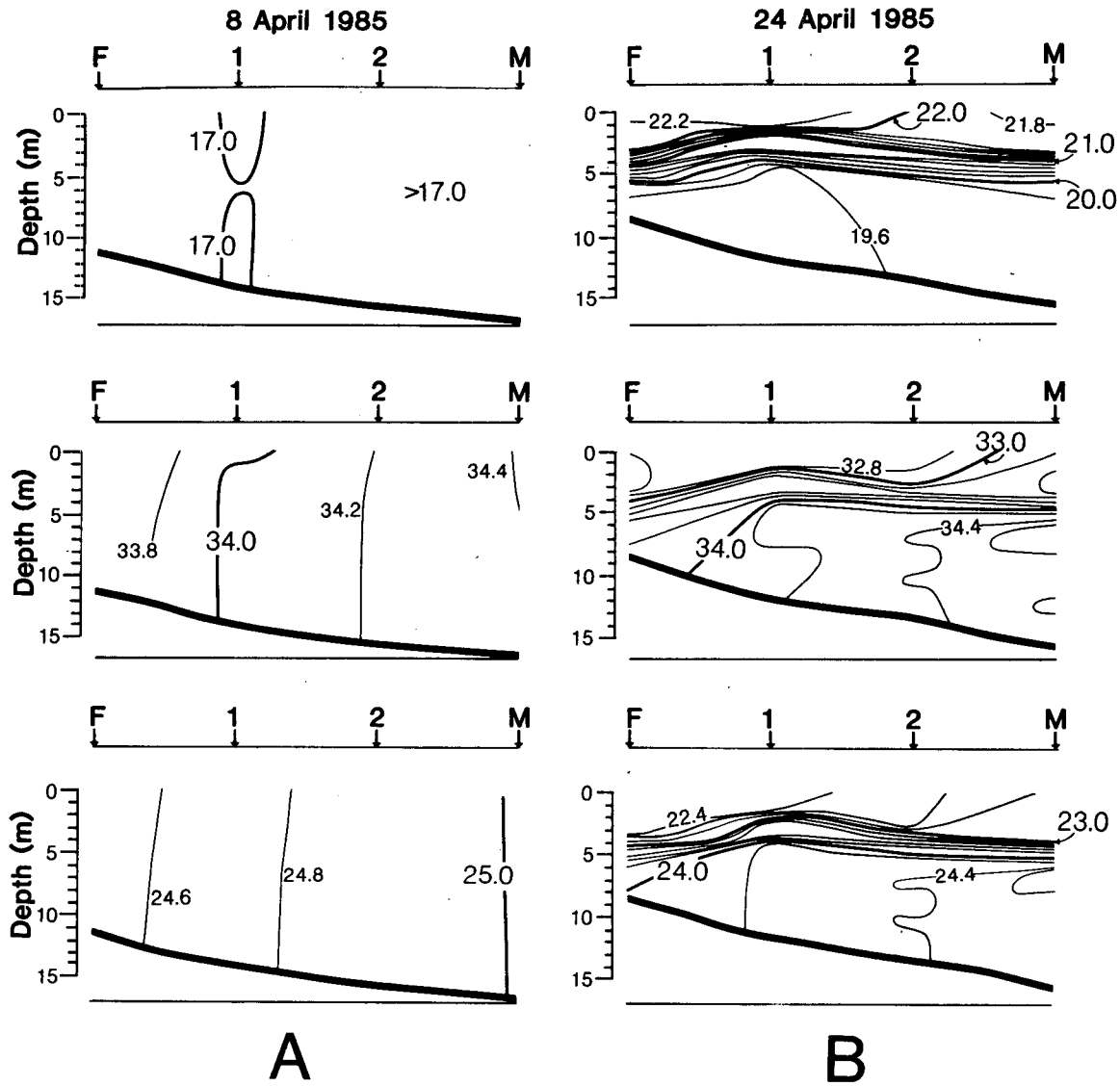

FIG. 3. Examples of hydrographic structure in the coastal frontal zone off Georgia. Panels display, from top to bottom, vertical sections of temperature, salinity and sigma-t along the F–M transect line. (a) 8 April, southwest wind stress, 0.4 dyn cm^{-2}; (b) 24 April, northeast wind stress, 0.6 dyn cm^{-2}.

within one data-point of being in phase. This finding agrees with previous studies (Schwing et al. 1985) showing that currents lag wind by 6 hours or less inside the 20-meter isobath off the southeastern United States.

The main results can be summarized as follows:

1) Mean currents within the frontal zone (along the 8-meter isobath) flow southward against the mean wind stress; seaward of the front, mean flow is northward;

2) There is a significant onshore component to the mean flow within 3 m of the bottom at all sites;

3) The most energetic fluctuations (from smallest to largest energy) in currents and wind stress occur at periods of 15, 2, and 5 days respectively.

The fluctuations in wind and current are statistically significant in these energy bands. Wind-generated currents in the 5-day band lag wind by about 6 hours.

5. Modeling studies

In order to gain further insight into the dynamics and thermodynamics of the wind-driven nearshore flows, a time-dependent x–z (cross-shore, depth) numerical model calculation was conducted using wind data obtained at Station T (Fig. 2). Model equations are the same as those used by Oey (1986; hencefore O86) and are not repeated here. All y-derivatives are dropped in the model equations and offshore bottom topographic variation is taken as that representative of Georgia–South Carolina inner and middle shelf regions

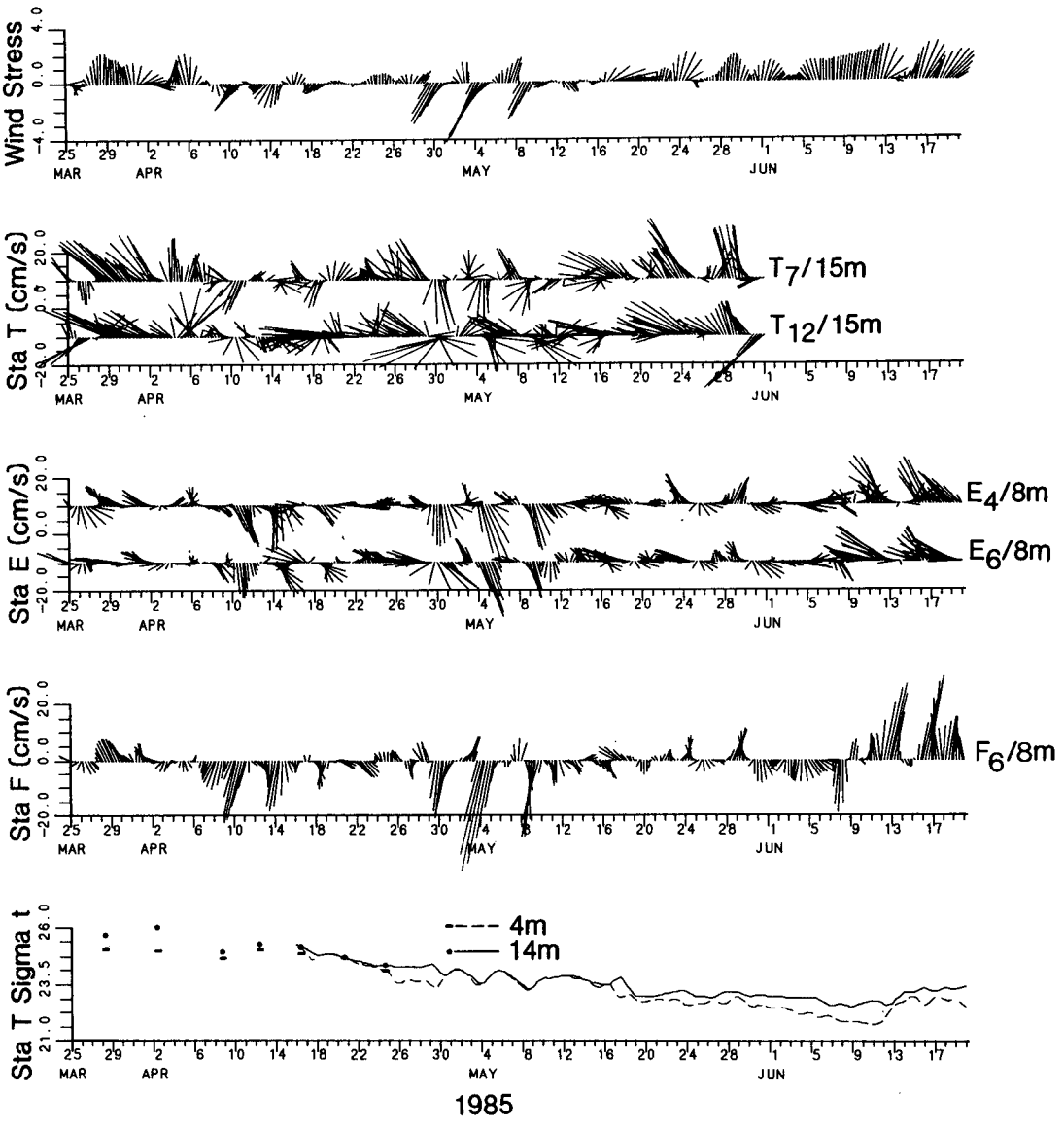

FIG. 4. Time series of 40-h low-passed winds, currents, and sigma-t (25 March–20 June 1985). All vectors were rotated −45 deg from east. The sigma-t values represented as dots at the beginning of the record are taken from cruise data.

(Fig. 7). Vertical mixing is calculated using Mellor and Yamada's (1982) level-2.5 turbulence closure scheme. Boundary conditions are (i) all fluxes, mass and heat, are zero at bottom boundary; (ii) "fresh" water influx with $S = 30‰$ is specified at the coast; (iii) wind stresses are specified at the ocean surface using the quadratic formulae and total downward heat flux as specified from climatology charts given in Kantha et al. (1986); and (iv) as in O86, standard open ocean boundary conditions are applied at the offshore boundary located at $x \approx 320$ km. Temperature and salinity are specified during inflow and are advected out using one sided differencing during outflow. The model ocean depth is constant at 500 m for 100 km $\leq x \leq$ 320 km where a coarse grid is used (O86). Thus one can view the near-shore region as being connected to a "reservoir" of ocean water further offshore. Sensitivity tests with the model show that errors introduced at the open ocean boundary have negligible effects on results in the near-shore region. Effects of tidal mixing near the bottom are directly computed by using Blumberg and Kantha's (1985) forced-wave radiation condition with an M_2 tidal amplitude of 0.4 m applied at the offshore boundary.

a. Model results

Initial conditions of the model correspond to 1 February 1985, when the water column is well mixed. The salinity and temperature fields are taken from clima-

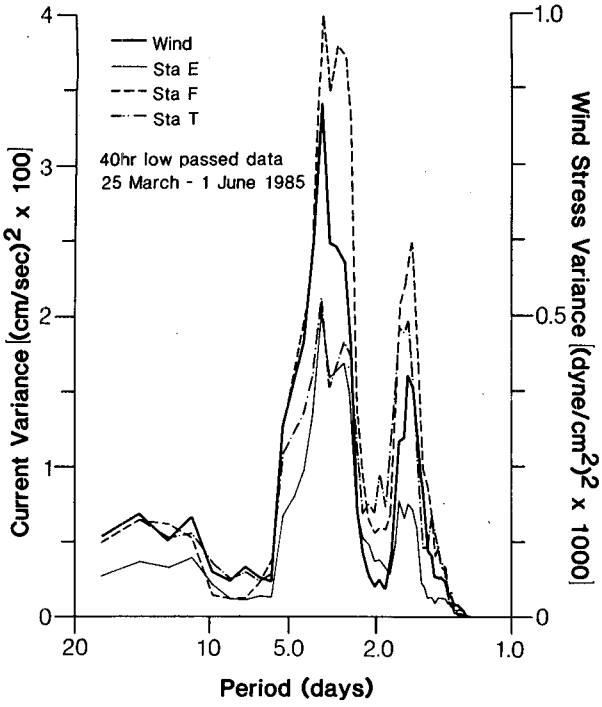

FIG. 5. Representative variance conserving spectra of the principal axes (rotated y-components) of wind stress and currents.

tology charts given in Kantha et al. (1986). Calculations were continued to cover the period from April through the end of May. Figure 7 shows a sequence of daily-averaged contours of σ_t and velocity vector plots, from 24 April through 1 May 1985. Winds are light and generally north-northeastward from 20 April through 27 April. From 24–29 April, nearshore upwelling, due to the wind forcing is evident. The water becomes stratified due to an offshore flow of less saline water near the surface and onshore return flow of dense water near the bottom. Observations (Fig. 4) also show the initiation of this stratification episode around 20 April. After a week of upwelling-favorable wind, the computed top to bottom σ_t difference at Station T increases to about 1.2 kg m^{-3} (Fig. 7, 27 April), in fair agreement with an observed value of about 1 kg m^{-3} (Fig. 4). Note that the model shows offshore advection of lenses of near-surface, less dense water, suggesting an efficient export of nearshore water at fairly low wind stresses $\sim$0.5 dyn cm^{-2}. The water in a bolus consists of coastal water which is vertically mixed in shallow water with offshore water brought inshore along the bottom in the cross-shelf component of the upwelling circulation. When wind reverses around the 30 April–1 May, the model shows downwelling (Fig. 7, 1 May) in the nearshore region and the water becomes well mixed. This feature also appears in the observed time series of sigma-t (Fig. 4) which shows the coalescence of near-bottom and near-surface sigma-t time series around 30 April–1 May. The ability to predict the onsets of stratification and/or mixing is an important feature of the present model. The wind-induced stratification/destratification events so computed (documented also by Oey et al. 1985 in a model simulation of estuarine circulation) depend on our use of a Richardson's number-dependent turbulence closure scheme and would not have been readily predicted by use of a constant eddy viscosity/diffusivity formulation.

After 1 May, observations indicate that isopycnals go through two relatively large amplitude fluctuations (Fig. 4), caused apparently by bursts of strong southwestward winds from 29 April–10 May. Model results

TABLE 3. Summary of means and kinetic energy of fluctuations of wind stress and current vectors off the Georgia coast (Fig. 2) in the 15-d, 5-d, and 2-d peaks of the spectra (Fig. 5). Wind stress (τ) units are in dyn cm^{-2} and currents are in cm s^{-1}. The energy values are based on summing the total energy density in a spectral analysis. All other variables present characteristics of rotary spectra for each of the vectors. Rotary coefficients are positive (negative) for cyclonic (anticyclonic) rotation. Angles represent the orientation of the major axis of the ellipse measured counterclockwise from east. Stability is a measure of the repeatability of elliptical parameters.

		τ	E_6	F_6	E_4	T_7	T_{12}
Mean	x	−0.05	−0.70	−0.37	0.93	−2.18	−3.65
	y	0.19	−0.79	−2.85	−0.88	3.08	1.18
Kinetic energy	Total	0.70	12.96	29.64	15.28	25.23	13.93
	15 d	0.13	2.29	5.00	3.04	4.77	3.04
	5 d	0.19	3.08	7.55	3.99	4.97	2.18
	2 d	0.05	0.92	3.08	1.07	2.63	1.22
Rotary coefficient	15 d	0.08	0.10	0.34	−0.04	−0.10	−0.52
	5 d	−0.22	0.03	−0.01	0.19	0.12	−0.21
	2 d	−0.02	−0.17	−0.10	−0.20	−0.01	−0.07
Angle	15 d	10	69	40	51	66	76
	5 d	19	68	35	54	56	73
	2 d	18	62	37	53	62	78
Stability	15 d	0.71	0.65	0.65	0.52	0.72	0.57
	5 d	0.45	0.56	0.89	0.70	0.73	0.49
	2 d	0.54	0.56	0.82	0.58	0.61	0.78

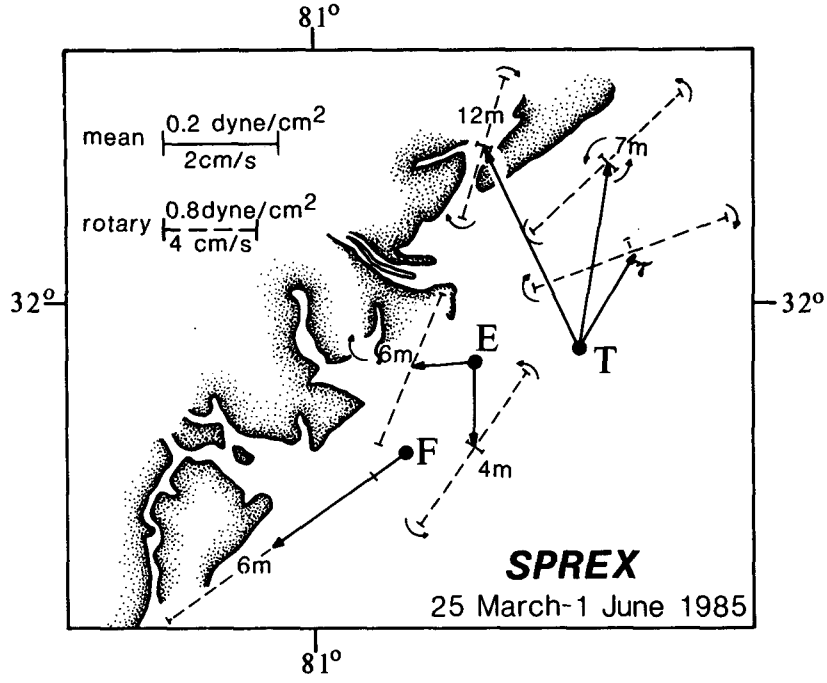

FIG. 6. Mean and oscillating wind and current vectors off the Georgia coast in the 5-day period band. Bold arrows represent means from 25 March to 1 June. The dashed lines represent the major/minor axes of 5-day oscillations about the mean.

(not shown) gave σ_t fluctuations of much smaller amplitude, and we suspect a strongly three-dimensional flow structure with significant contribution from the $\partial v/\partial y$ term. One also wonders if inclusion on an alongshore pressure gradient $\rho_o^{-1}\partial p/\partial y$ (as external forcing to the 2-D model), as questioned by one anonymous reviewer, would change the model results. We suspect that it would not, for two reasons. First, $\rho_o^{-1}\partial p/\partial y$ will be shown in section 6 to be about 10^{-6} m s^{-2} inside the nearshore front. In a water depth of about 10 m, this will contribute about 0.1 dyn cm^{-2}, or about 10%, to a typical wind stress of 1 dyn cm^{-2} during the experiment. The shelf region along the U.S. southeast coast is typically shallow and gently-sloping (10–30 m over 100 km, Fig. 1) and inclusion of $\rho_o^{-1}\partial p/\partial y$ in a simple 2-D model would not produce significantly different results.

TABLE 4. Coherence-squared and phase relations between alongshore components of wind and current off the Georgia coast (Fig. 2) in the 5-day band. When phase lag is positive, the left-hand parameters lead. Coherence-squared values greater than 0.46 are statistically significant.

	5-day band	
Parameter	Phase lag (h)	Coherence squared
τ vs E_6	5	0.87
τ vs F_6	2	0.92
τ vs E_4	3	0.95
τ vs T_7	8	0.86
τ vs T_{12}	7	0.70
E_6 vs F_6	−4	0.92
E_6 vs E_4	−2	0.91
E_6 vs T_7	3	0.87
E_6 vs T_{12}	0	0.70
F_6 vs E_4	1	0.95
F_6 vs T_7	6	0.86
F_6 vs T_{12}	5	0.72
E_4 vs T_7	4	0.90
E_4 vs T_{12}	3	0.77
T_7 vs T_{12}	0	0.73

Second and more important, such inclusion would not be meaningful in the present case. We will show in section 6 that $\rho_o^{-1}\partial p/\partial y$ changes sign across the frontal zone and is approximately equal to -10^{-6} m s^{-2} just outside the frontal zone at the 15 m isobath. This represents a decrease in $\rho_o^{-1}\partial p/\partial y$ of about 2×10^{-6} m s^{-2} over a cross-front scale of about 10 km, or $\rho_o^{-1}\partial^2 p/\partial x\partial y \approx -2 \times 10^{-10}$ s^{-2}. If the alongshore velocity "v" is assumed to be in geostrophic balance with the cross-shore pressure gradient (a good approximation): $\rho_o^{-1}\partial p/\partial x = fv$, one obtains $\rho_o^{-1}\partial^2 p/\partial x\partial y = \beta v + f\partial v/\partial y$. With "$v$" of O(0.1 m s^{-1}), contribution from the beta term $\beta v \approx$ O(10^{-12} s^{-2}) is negligible, so that $\partial v/\partial y \approx -2 \times 10^{-6}$ s^{-1}. This represents a 0.1 m s^{-1} change in "v" in an alongshore distance of only 50 km, comparable to a mean magnitude of about 5×10^{-6} s^{-1} for $\partial u/\partial x$ during the observation period (Table 2). Thus three-dimensionality is important in the present observations of a nearshore frontal zone involving active interaction of

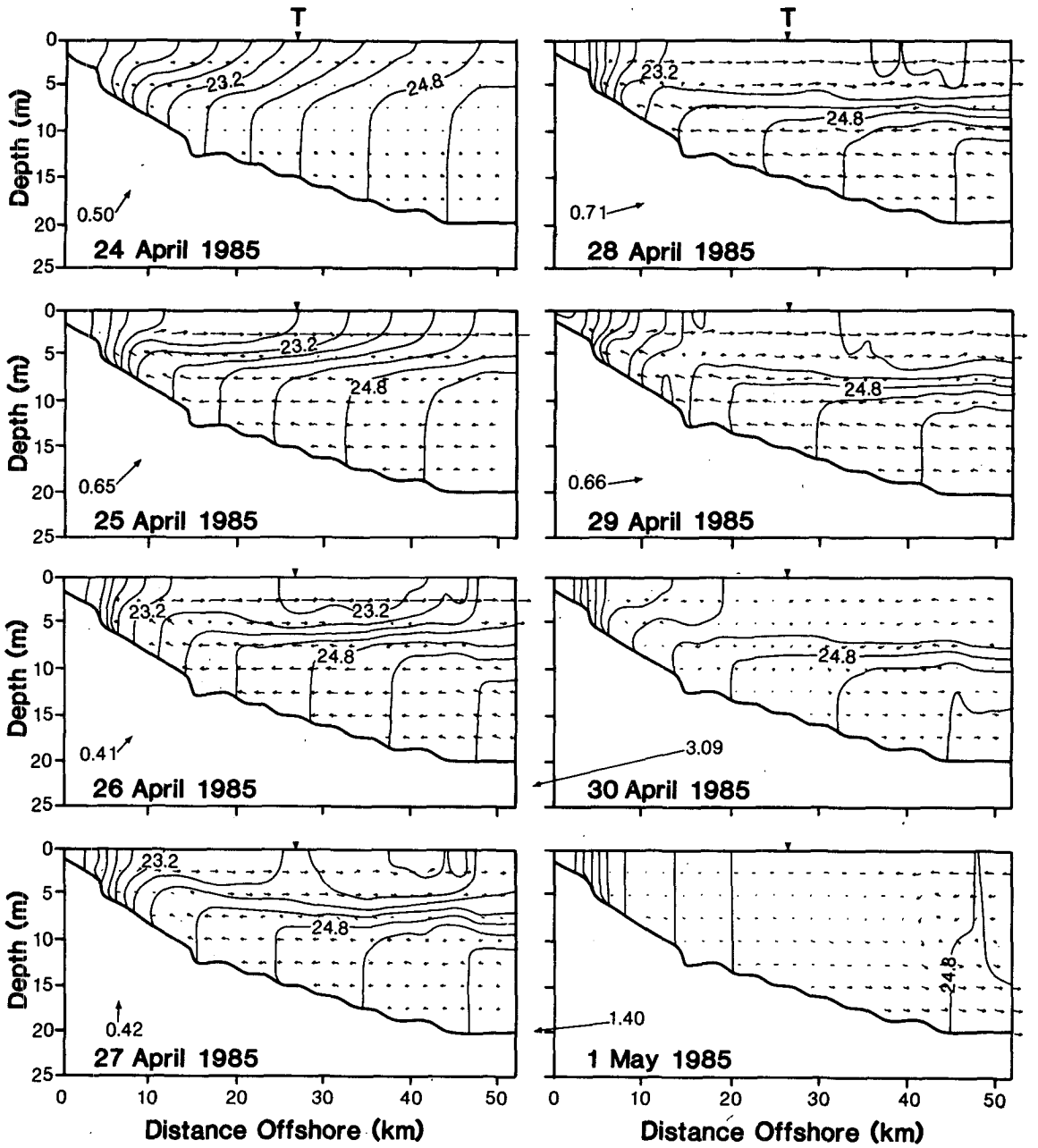

FIG. 7. Daily-averaged contours of σ_t superimposed on cross-shelf velocity vector plots from a two-dimensional model using wind data observed off Savannah, Georgia. Daily-averaged wind stress (dyn cm^{-2}) is plotted at lower left. Isopycnals are plotted at 0.4 intervals in σ_t.

river plumes and frontal eddies. Any attempt to stretch the 2-D model beyond the simple interpretations of wind-induced stratification/destratification events described here, by ad-hoc inclusions of alongshore pressure gradients for example, would be of doubtful usefulness. A better approach is to extend the 2-D model to a fully three-dimensional model and combine the results with observations to better understand the three-dimensional flow structure of the nearshore front. This work is currently in progress and will be reported in a separate paper (Oey and Blanton 1988).

b. Interpretation of model results

Model results illustrate the importance of vertical mixing and wind-induced advection in modifying the structure of coastal frontal zones (Fig. 8), as was first

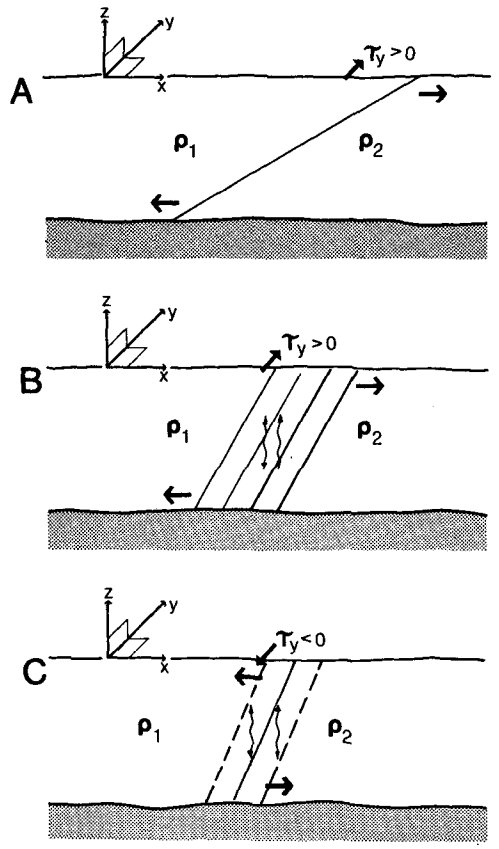

FIG. 8. (a) Differential tilting of front due to positive alongfront wind stress, in the absence of vertical mixing; (b) as in (a) but with vertical mixing represented by the wavy arrows, which tend to diffuse the front; (c) differential tilting of front due to negative alongfront wind stress. Tilting cannot occur indefinitely in nature without some vertical mixing.

stressed by Blanton (1981) for the South Atlantic Bight nearshore regions. Oey 1986 also considered wind-induced formation and maintenance of continental shelf fronts in the SAB during winter. Indeed, many aspects of the postulated frontal dynamics O86 are also directly applicable to the present case. The dynamic similarities between a shelf-break front and a shallow coastal front in waters of the southeastern United States can be summarized as follows:

1) buoyancy is continuously supplied by relatively warm Gulf Stream water (O86) and freshwater discharges from rivers (Blanton 1981);
2) along-front wind stress induces differential advection in the cross-front-depth plane in the presence of a cross-frontal density gradient;
3) vertical mixing, by either wind work on the water surface, tidal work near the bottom, or density overturnings due to advection and atmospheric cooling alters the shape of the frontal zone.

c. Syntheses of observations and model results

During the seven cruises conducted from 29 March to 25 April, net heat input through the sea surface and discharge from the Savannah River provided the major sources of buoyancy which inhibited the ability of wind stress to homogenize the water column in the frontal zone. We calculated that climatological net heat additions for a two month period encompassing the cruise period should be about -30 W m^{-2} (Kantha et al. 1986) which translates to a buoyancy flux of O(10^{-8}) m^2 s^{-3}. The corresponding average wind power measured at Station T was about O(10^{-3}) W m^{-2} which is about 10^{-6} W m kg^{-1} on a unit mass basis.

The Monin–Obukhov mixing length (L_v) for these values (Phillips 1966) is

$$L_v = \frac{W/\rho}{\kappa N(0)} = \mathrm{O}(200\ \mathrm{m})$$

where $N(0)$ is buoyancy flux at the sea surface, W is the wind power and $\kappa = 0.42$. Here L_v is clearly too large and there must be an additional source of buoyancy that would limit L_v to O(1 m) or O(10 m). Local freshwater discharge is the obvious source. The average Savannah River discharge (Q_r) one month before the cruises (Blanton and Atkinson 1983) was about 200 m^3 s^{-1}. An estimate of the area of influence of fresh water over the inner shelf is O(LW_c), where W_c is the cross-shore width of influence and L is the alongshore length of influence $L \approx 2\pi\mathrm{Ro}$, an estimate of the circumference of the inertial circle traced by Savannah River plume as it discharges onto the continental shelf. This, incidently, is also the scale of the along-front meander wave of density-driven boundary currents (Griffiths and Linden 1982). With Ro, the baroclinic Rossby radius, $\approx$ 10–20 km, we obtain

$$N(0) = \frac{g}{\rho}\left[\frac{\rho Q_r}{LW_c}\right] = \mathrm{O}(10^{-6}\ \mathrm{m^2\ s^{-3}}).$$

Thus, $N(0)$ due only to this freshwater source is two orders of magnitude greater than $N(0)$ due to heat energy only. Using this value for the estimate of $N(0)$, L_v = O(1 m) is more reasonable in view of the observations of stratification during the seven cruises.

Models employing L_v are useful as long as advection of buoyancy is unimportant. A test of this model would be to plot wind work against potential energy PE (Table 5). Here, we follow Simpson and Bowers (1981) to define PE as the potential energy of the water column relative to its well-mixed state:

$$\mathrm{PE} = \int_{-h}^{0} [\rho - \langle\rho\rangle]\, gz dz \qquad (5.1)$$

where ρ is the in situ density and the angle brackets denote a depth average, i.e.

$$\langle\rho\rangle = \int_{-h}^{0} \rho dz/h. \qquad (5.2)$$

TABLE 5. Summary of energy terms for seven cruises during the period 26 May–24 April. Wind stress components are cross-shelf (X) and alongshelf (Y). Estimates for wind work are based on time integral of wind power at Station T. Integrals were computed over a 1.5-day period before the end of each cruise. Potential energy (PE) using the formula of Simpson et al. (1978) and heat content (HC) are calculated from surface area and water column integrals of hydrographic station data (Fig. 3). PE data have been divided into PE of entire domain (a) and PE of outer three stations (b).

Cruise	Date	Wind stress* (N $M^{-2} \times 10$)		HC (J $M^{-2} \times 10^6$)	Wind work (J M^{-2})	PE (J M^{-2})	
		X	Y			(a)	(b)
0	28 Mar	−0.078	1.639	724	740	−163	−129
1	2 Apr	1.227	0.119	765	380	−190	−284
2	8 Apr	0.102	−0.128	819	34	−34	−22
3	12 Apr	−0.391	−0.029	804	75	−60	−51
4	16 Apr	−0.120	0.481	803	140	−180	−121
5	20 Apr	−0.215	0.130	884	28	−119	−31
6	24 Apr	−0.082	0.634	951	110	−290	−343

* Averages using 3HLP data with Dt = 1 h.

Thus, the stratification state of the water column at a horizontal position (x, y) and time t, depends on the value of PE; it is well-mixed when PE = 0 and stratified when PE is negative. A successful test would therefore show that increased work leads to increased potential energy. An examination of the data (Table 5) will show that this test would fail. In fact higher potential energy occurred when wind work was relatively small (Cruises 2, 3 and 5). Thus, advection of buoyancy appears to be important, as suggested by the 2-D model results of the previous section. To include the effects of buoyancy advection we use the following expression for the time rate of change of PE as derived by Van Aken (1986) and Oey et al. (1987)

$$(\mathrm{PE})_t \approx \rho_a C_{oa} C_a |\mathbf{u}_a|^3 + \rho_o C_{ob} C_b |\mathbf{u}_T|^3 + (gh/2)\cdot[\alpha Q/C_{pw} + \beta S_0(E_v - P_r)] - g(d\langle\rho\rangle/dx)\tau_0{}^y h/(f\rho_o), \quad (5.3)$$

where $\mathbf{u}_a = (u_a, v_a)$ is the wind velocity vector, $\mathbf{u}_T = (u_T, u_T)$ is the tidal velocity vector, C_a and C_b are the wind and bottom drag coefficients, respectively, with values of about 2×10^{-3}, $C_{oa} \approx \mathbf{u}(x, y, z = 0, t)/\mathbf{u}_a$, $C_{ob} \approx \mathbf{u}(x, y, z = -h, t)/\mathbf{u}_T$, $\mathbf{u} = (u, v, w)$ is the fluid velocity vector, ρ_a and ρ_o are reference air and ocean densities respectively, $\alpha = -(\partial\rho/\partial T)/\rho \approx 2 \times 10^{-4}\ \mathrm{K}^{-1}$, $\beta = (\partial\rho/\partial S)/\rho \approx 8 \times 10^{-4}$, where Q is the total heat flux across the air–sea interface in W m^{-2}, positive upward, C_{pw} the specific heat for water $\approx 4 \times 10^{-3}$ J kg^{-1} K^{-1}; S_0 is the near-surface ocean salinity in parts per thousand; $(E_v - P_r)$ is the rate of evaporation minus precipitation, in kg m^{-2} s^{-1}; $\tau_0{}^y$ is the alongshore wind stress, and f is the Coriolis parameter.

The simplifying assumptions made in deriving (5.3) are (Van Aken 1986; Oey et al. 1987) (i) horizontal advection of density is predominantly in the cross-frontal (x) direction and (ii) horizontal advection is Ekman-induced wherein a northward (southward) wind stress transports surface water offshore (onshore) and a compensating onshore (offshore) transport is produced in the lower layer (Fig. 9). Note that contribution to $(\mathrm{PE})_t$ in (5.3) from the vertical velocity component involves the integral

$$\int_{-h}^{0} [w - \langle w\rangle] z dz,$$

which is identically zero for a w-distribution symmetrical with z about $z = -h/2$. Implicit in (5.3) is also the condition that $|\delta\tau_0{}^y/\tau_0{}^y|$ is small. In the nearshore zone under steady (or quasi-steady; time scale $\gg 1/f$) conditions, $\rho_o{}^{-1}|\delta\tau_0{}^y| \sim |h\rho_o{}^{-1}\partial\rho/\partial y| \sim 10^{-6}$ m^2 s^{-2}, using estimates of the values of $\partial\rho/\partial y$ obtained from observations (see section 6). The condition is therefore satisfied except for very low wind stresses of less than 0.1 dyn cm^{-2}, a wind stress regime in which wind-induced advection is unimportant.

We now nondimensionalize (5.3) by assuming a quadratic aerodynamic law for τ_0:

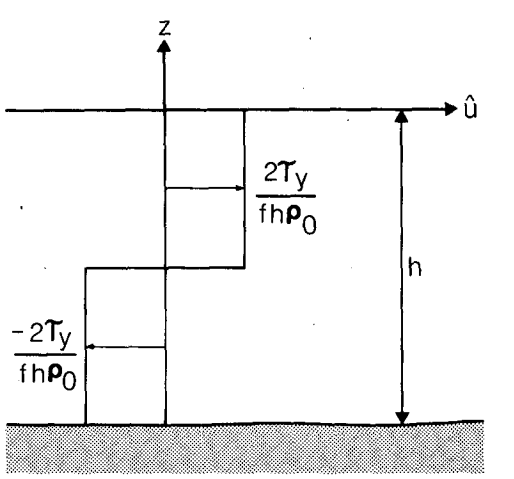

FIG. 9. The velocity shear generated by a positive wind stress τ_0.

$$\tau_0{}^y = \rho_a C_a |\mathbf{u}_a| v_a,$$

substitute this into (5.3), take a time average of the resulting expression over a period Δt (denoted by overbar) and then divide through by $\rho_a C_a |\mathbf{u}_a|^3$, obtaining:

$$\frac{(\Delta(\mathrm{PE})/\Delta t)}{(\rho_a C_a |\mathbf{u}_a|^3)} \approx C_{oa} + (\rho_o/\rho_a) C_{ob}(C_b/C_a) \frac{|\mathbf{u}_T|^3}{|\mathbf{u}_a|^3} + (gh/2)\cdot [\alpha \bar{Q}/C_{pw} + \beta \bar{S}_0(\bar{E}_v - \bar{P}_r)]/(\rho_a C_a |\overline{\mathbf{u}_a}|^3) - \frac{d\langle \bar{p} \rangle}{dx}\cdot\frac{(gh)^{1/2}}{\rho_o f}\cdot\left[(gh)^{1/2}\frac{|\overline{\mathbf{u}_a}|\,|\overline{v_a}|}{|\overline{\mathbf{u}_a}|^3}\right] \quad (5.4)$$

The physical interpretation of (5.3), or (5.4) is straightforward. Wind and tidal work "stir" up the water toward a well-mixed state and hence tend to increase the potential energy of the water column. Heating of the ocean surface (negative Q) and precipitation increase its stratification and hence tend to decrease the potential energy of the water column; cooling and evaporation have the opposite effect. Positive alongshore wind stress (with positive offshore density gradient) transports less dense nearshore water offshore in the surface layer and induces compensating onshore flow of denser sea water, and decreases the potential energy of the water column which increases its stratification. Negative alongshore wind stress has the opposite effect. The last term of 5.3 and 5.4 also illustrates the dual role played by alongshore wind stress which, on one hand, induces stratification by advection, and on the other hand, vertically mixes the water column. These scenarios of stratification and homogenization events are borne out in our model results described previously (Fig. 7).

d. *Correlation of wind work with changes in potential energy*

We can test the validity of Eq. (5.4) with observations of wind work at Station T. We have used data from Fig. 4 to plot $|u_a| v_a (gh)^{1/2}/(|u_a{}^3|)^2$ and $[d(\mathrm{PE})/dt]/\rho_a C_a |u_a|^3$ as a function of time (Fig. 10). To calculate potential energy, we assumed a linear vertical distribution of ρ

$$\rho = az + b,$$

where

$$a = -(\rho_2 - \rho_1)/(h_2 - h_1)$$

$$b = (h_2\rho_1 - h_1\rho_2)/(h_2 - h_1)$$

$$\rho = \rho_i \quad \text{at} \quad z = -h_i, \quad i = 1, 2.$$

Then

$$\mathrm{PE} = agh^3/12.$$

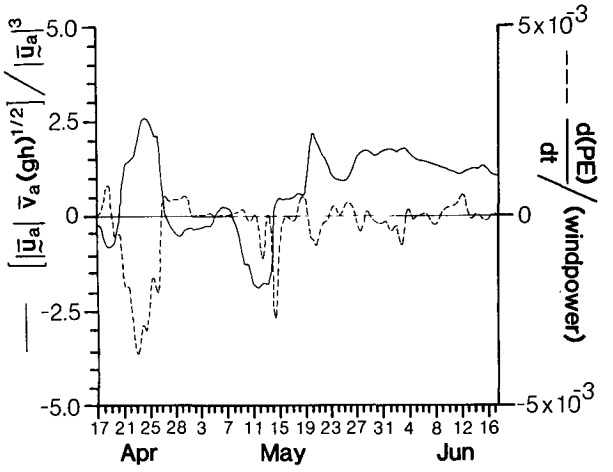

FIG. 10. Plot of nondimensional variables in Eq. (5.4) vs time using data from Fig. 4. Data have been averaged 4 days backward in time and applied to the rate of change in PE over that time interval.

For a two-layer fluid system where

$$\rho = \begin{cases} \rho_1, & -ah < z \leq 0 \\ \rho_2, & -h \leq z < -ah, \quad 0 < a < 1 \end{cases} \quad (5.5)$$

$$\mathrm{PE} = gh^2(\rho_2 - \rho_1)a(a-1)/2. \quad (5.6)$$

The data have been averaged 4 days backward in time. Note that due to changes in the mean stratification produced by variation in surface heat input over the two-months observational period, $d\langle\rho\rangle/dx$ varies also and $(\mathrm{PE})_t$ would not be a simple linear function of $\tau_0{}^y$ as implied by (5.3). Nonetheless, the plot in Fig. 10 shows fairly good correlation between stratification and alongshore wind stress for isolated time periods. It also suggests that $\Delta\rho$ is affected by buoyancy inputs (either from the surface or due to alongshore buoyancy variation), that may isolate subsurface waters from the direct effect of wind stress. During the time interval 17 April–15 May, the changing wind stress is reflected in changes in PE as predicted by the model simulations and by (5.4). The episodes of positive stress (20–27 April) coincided with large decreases in PE, and the negative stress (17–20 April) coincided with increases in PE. The episode of negative stress during 8–14 May was accompanied by decreases in PE suggesting that buoyancy was advected in from the alongshore direction, which would violate the assumption of negligible alongshore gradients used in simulations and in the derivation of (5.3).

After 15 May, conditions became more complex but correlation between the two curves about some nonzero mean can still be seen. We do not know the distribution of low salinity water during this period, but it seems reasonable that the relatively persistent alongshore wind stress northward tilted the front almost horizontally so that $\partial\rho/\partial x \approx 0$. Moreover, solar radiant energy

was approaching its annual maximum, and the amount of possible sunshine was high and persistent after 24 May (from cloud cover and sunshine data at Savannah airport). These conditions would combine to inhibit the work performed by wind stress after 24 May.

It would be incorrect to test (5.4) directly using the cruise data in Table 5 because the time intervals between cruises are of O(5 days), during which PE fluctuates significantly. Instead, we integrate (5.4):

$$\mathrm{PE}(t) = \mathrm{PE}(t - \Delta t) + \int_{t-\Delta t}^{t} [\rho_a C_{oa} C_a |\mathbf{u}_a|^3 + \rho_o C_{ob} C_b |\mathbf{u}_T|^3] dt + \frac{1}{2} gh \int_{t-\Delta t}^{t} [\alpha Q / C_{pw} + \beta S_0 (E_v - P_r)] - \frac{gh(d\langle\rho\rangle/dx)}{\rho_o f} \int_{t-\Delta t}^{t} - \tau_0{}^y dt$$

where Δt is an appropriate averaging time for wind stress and t is the time at the middle of the cruise. Elapsed time for each cruise was about 16 hours. We have plotted the average alongshore wind stress against PE(t) (Fig. 11). Averaging time for wind stress is 1.5 days and is based on the lag time over which the autocorrelation of a sinusoid goes to zero (¼ wave period). For the approximate 6-day period peak in wind and current energy observed in wind stress (Fig. 5), the quarter-wave period = 1.5 days. The data indicate a tendency for decreased potential energy as wind stress increases (positive) especially for stresses below 0.6 dyn cm^{-2}. Thus, advection and consequent lowering of potential energy would be proportional to wind stress (Figs. 10 and 11). We suspect, however, that increased vertical mixing at high wind stress would compensate for the advection of buoyancy, and potential energy would begin to increase ($\Delta\rho$ would decrease) at some point. This is also suggested by the data (Fig. 11, Cruise 0).

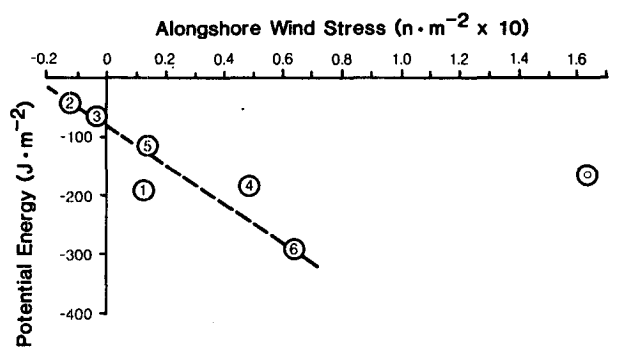

FIG. 11. Relationship of alongshore wind stress to potential energy for seven cruises conducted from 28 March to 24 April, 1985 (see also Table 5). Stress data are plotted as 3-h low-passed values averaged for 1.5 days before the end of each cruise. Dotted line is fitted by eye. See text for details.

6. Alongshelf advection

Mean currents within the frontal zone flowed southward against the mean wind stress (Fig. 6). Seaward of the front, mean flow was northward. We examined this finding by partitioning the wind stress record (Fig. 4) into 21 events and plotted the average wind stress against the average current for each event (Fig. 12). We related the slope and y-intercept of linear regression lines fitted to these data to a linearized bottom drag coefficient (r) and the alongshore pressure gradient force (Table 6) in a manner similar to that described by Scott and Csanady (1976). However, we plotted wind stress as the independent variable. Reversing the x- and y-axis variables changes the value of r and pressure gradient force by less than 20%. See appendices A and B for more details.

The values of $r \approx 1.5$–3 ($\times 10^{-3}$) m s^{-1} obtained from these regression plots are larger than those obtained by Atkinson et al. (1983), $r_A \approx 10^{-3}$ m s^{-1}. To match coastal sea level and current meter observations under homogeneous conditions during autumn in the nearshore region off South Carolina, we deduced from a barotropic model analysis that $r = r_s \approx 3.7 \times 10^{-4}$ m s^{-1} (Schwing et al. 1985). We attributed this reduction to effects of a wind-induced, oscillating alongshore pressure gradient (cf. Beardsley and Winant 1979). We suspect that the present value of r is too large because of effects of oscillating alongshore pressure gradient, as well as effects of vertical stratification. Stratification is expected to be significant in the present observations of the coastal salinity front during spring and early summer. Due to baroclinicity, a given wind stress would induce a reduced current in the lower portion of the water column, thereby reducing the slopes of the regression lines (Fig. 12) more than would be the case for barotropic (unstratified) conditions. This has the effect of falsely enhancing bottom drag, an effect that should be more apparent for current meters located near the bottom of the water column. This may account for the fact that the slopes of regression line for T_{12} and E_6 are smaller than those for T_7 and E_4 (Fig. 12).

Using the equation in appendix A and using the value of "r" as deduced from Fig. 12 gives (Table 6),

$$\mathrm{PGF}_y = \frac{1}{\rho_o}\frac{\partial p}{\partial y} \approx -2.0 \times 10^{-6} \text{ m s}^{-2} \quad \text{at Station T}$$

$$\approx 5.3 \times 10^{-6} \text{ m s}^{-2} \quad \text{at Stations E and F.}$$

We believe that the sign change in $\rho_o{}^{-1}\partial p/\partial y$ across the frontal zone is correct. Thus, the intercepts at $\tau_0{}^y = 0$ axis in Fig. 12 are also correct, reflecting merely the oppositely-flowing mean currents inside and outside the front as shown is Fig. 6. The magnitudes of $\rho_o{}^{-1}\partial p/\partial y$ are unreasonably large, however. Sturges

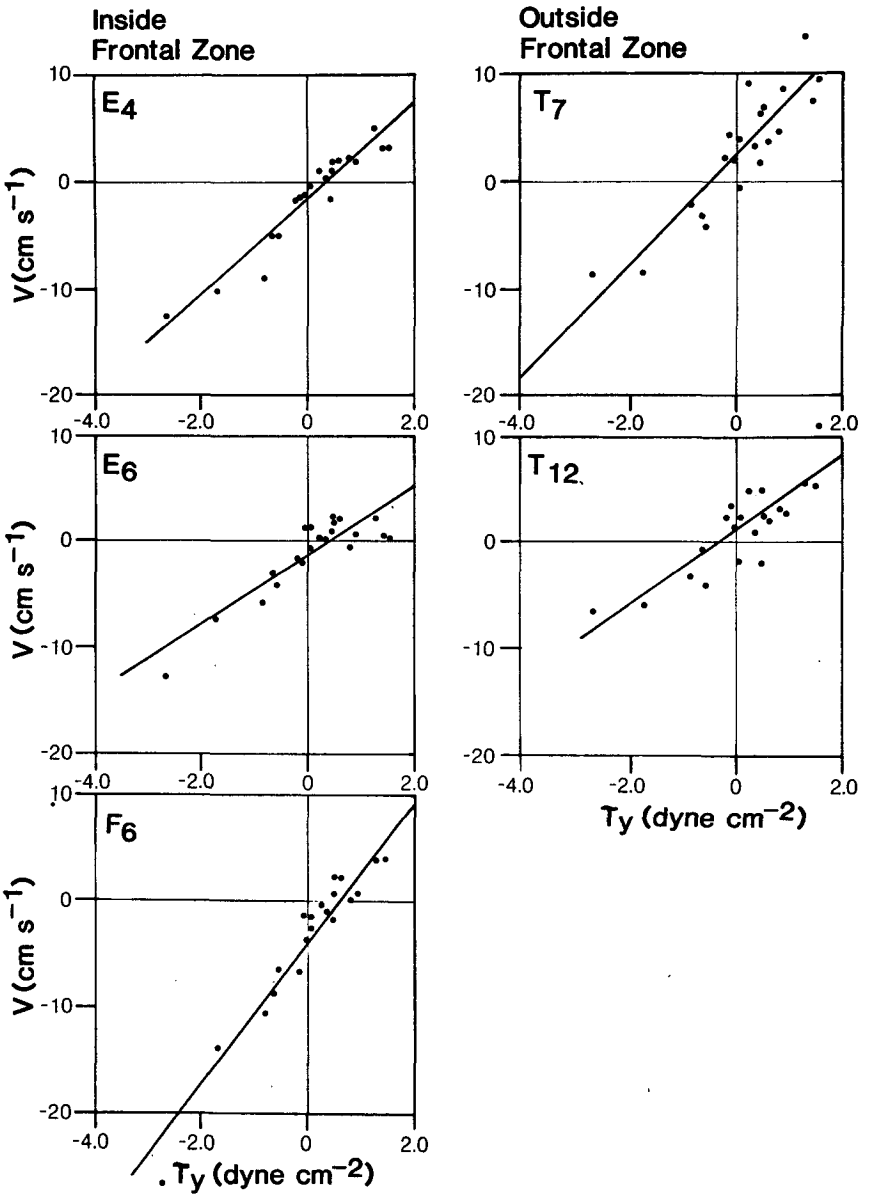

FIG. 12. Plots of 40-h low-passed alongshore components of currents vs wind stress (averaged by event) for 21 events from 27 March to 1 June 1985. Regression results are summarized in Table 6.

(1974) and Lee et al. (1985) estimated that sea level slope along the Gulf Stream $(\partial\xi/\partial y)_{GS} \approx -2 \times 10^{-7}$ and therefore $(\rho_o^{-1}\partial p/\partial y)_{GS} \approx -2 \times 10^{-6}$ m s^{-2}. Thus, $\rho_o^{-1}\partial p/\partial y$ increases onshore since it changes sign across the nearshore frontal zone. The value of $(\rho_o^{-1}\partial p/\partial y)_T \approx -2.0 \times 10^{-6}$ m s^{-2} at Station "T", located at a distance of only 20–30 km from the shore, is comparable in magnitude to $(\rho_o^{-1}\partial p/\partial y)_{GS}$. This is surprising since one would expect that, with influence of northward winds and fresh water, $|(\rho_o^{-1}\partial p/\partial y)_T/(\rho_o^{-1}\partial p/\partial y)_{GS}|$ would be small.

The values $(\rho_o^{-1}\partial p/\partial y)_{E,F} \approx 5.3 \times 10^{-6}$ m s^{-2} at Stations E and F are also unreasonably large. The implied cross shore rate of decrease of $\rho_o^{-1}\partial p/\partial y$ across a frontal zone of about 10 km width is $\rho_o^{-1}\partial^2 p/\partial x\partial y \approx -7 \times 10^{-10}$ s^{-2}. Thus, (cf. section 5a) $\partial v/\partial y \approx (\rho_o f)^{-1}\partial^2 p/\partial x\partial y \approx -10^{-5}$ s^{-1}, a change of v of about 0.5 m s^{-1} over an alongshore distance of only 50 km! While such a large change could occur within short time scales of 1–2 days, we doubt that such spatial changes are correct over a time-mean of O(weeks–months). Therefore in subsequent calculations, we will reduce r to $r_s \approx 3.7 \times 10^{-4}$ m s^{-1} given in Schwing et al. (1985). As a result

TABLE 6. Results of regression of alongshore components of wind stress and currents from each current meter located in Fig. 2. The R^2 is the square of the linear correlation coefficient. Using the vertically averaged alongshore momentum balance as a model, the slope is related to a linear resistance coefficient, r; the y-intercept is related to an alongshore pressure gradient force (PGF_y). (See appendix A). Numbers in the second column of PGF_y were calculated using $r = 3.7 \times 10^{-2}$ cm s^{-1} given in Schwing et al. (1985). See text for details.

Location/depth (m)	Water depth (m)	Slope of line	yi (cm s^{-1})	R^2	r (cm s^{-1})	$C_D \times 10^3$	$PGF_y \times 10^4$ (cm s^{-2})	
F/−6	−8	6.57	−3.93	0.88	0.15	2.4	6.64	1.64
E/−4	−8	4.41	−1.50	0.92	0.22	2.0	4.24	0.71
E/−6	−8	3.32	−1.30	0.79	0.30	2.7	4.90	0.60
T/−7	−15	5.21	2.22	0.84	0.19	3.6	−2.86	−0.56
T/−12	−15	3.22	0.59	0.77	0.30	4.8	−1.20	−0.15

$$PGF_y = \frac{1}{\rho_o}\frac{\partial p}{\partial y} \approx \begin{cases} -0.4 \times 10^{-6} \text{ m s}^{-2} & \text{at Station T} \\ +1.0 \times 10^{-6} \text{ m s}^{-2} & \text{at Stations E and F.} \end{cases}$$

The revised values of PGF_y are found in the right-most column of Table 6.

Thus, the alongshore pressure gradient forced over the continental slope/outer shelf by the Gulf Stream $\left(\left[\frac{1}{\rho_o}\frac{\partial p}{\partial y}\right]_{GS} \approx -2 \times 10^{-6} \text{ m s}^{-2}\right)$ increases (i.e., decreases in magnitude) onshore, and even changes sign as one approaches close to the coast. We suggest that the increase is due to sea-level setup over the South Atlantic Bight, caused primarily by spring/summertime south/southwesterly winds, and perhaps also by uneven freshwater discharge along the coast. The setup is directed opposite to the setup along the Gulf Stream.

We examined the data (Fig. 12, Table 6) by analyzing the momentum balance (using $r_s = 3.7 \times 10^{-4}$ m s^{-1}) within and outside the frontal zone when wind stress is absent. The steady-state, linearized cross-shelf and alongshelf momentum equations are

$$-fv = -\frac{1}{\rho_o}\frac{\partial P}{\partial x} + \frac{\partial \tau_x}{\partial z} \tag{6.1a}$$

$$fu = -\frac{1}{\rho_o}\frac{\partial P}{\partial y} + \frac{\partial \tau_y}{\partial z} \tag{6.1b}$$

where P is pressure, τ_x and τ_y are components of internal (kinematic) stress, ρ_o is a reference density and the remainder of the terms have already been defined.

a. *Momentum balance outside the frontal zone*

The y-intercept in Fig. 12 for Station T is $v(x_T, y, z)$. We assume that contribution from $\partial\rho/\partial y$ is small outside the frontal zone and estimate a barotropic part of $v(x_T, y, z)$ by vertically integrating (6.1b). Thus, since the vertically averaged cross-shelf component of velocity (U) is small near the coast:

$$\tau_b{}^y = rv_o = -gh\frac{\partial \xi}{\partial y} \tag{6.2}$$

where $\tau_b{}^y = rv_o$ is the alongshelf component of bottom stress, r is the linearized drag coefficient, h is bottom depth, and ξ is sea-surface elevation. With $r \approx 3.7 \times 10^{-4}$ m s^{-1}, $h \approx 15$ m and the y-intercept $y_i \approx v_o \approx 0.02$ m s^{-1} we obtain $\partial\xi/\partial y \approx -5 \times 10^{-8}$, or $g\partial\xi/\partial y = -0.5 \times 10^{-6}$ m s^{-2}.

A rough estimate of the wind-induced static setup is $g\partial\xi/\partial y \approx \tau_0{}^y/h \approx 1.3 \times 10^{-6}$ m s^{-2} for a mean (kinematic) wind stress of 1.9×10^{-5} m^2 s^{-2} (Table 3) and water depth at Station T, ≈ 15 m. Subtracting this component of the pressure gradient from $(\rho_o{}^{-1}\partial p/\partial y)_{GS} \approx -2 \times 10^{-6}$ m s^{-2}, we obtain $(\rho_o{}^{-1}\partial p/\partial y)_T \approx -0.7 \times 10^{-6}$ m s^{-2} at Station T which compares with a value of -0.5×10^{-6} m s^{-2} calculated above.

The slope of -5×10^{-8} outside the frontal zone can also be compared with a calculated slope of -2.9×10^{-7} for autumn in the same region (Blanton 1981), when winds are generally southward. Sea level slope for the autumn case was attributed to either the slope along the Gulf Stream $(\partial\xi/\partial y)_{GS}$ and/or to wind-driven setup $(\partial\xi/\partial y)_{WIND}$ along the Florida coast.

b. *Momentum balance inside the frontal zone*

The mean alongshelf flow inside the frontal zone consists of three parts driven by separate terms of the momentum balance. The first part is that driven by $\partial\xi/\partial y$ which has been calculated already and which at the 8 m isobath would drive a northward flow v_o of about 10^{-2} m s^{-1}. The second part results from the cross-shore density gradient inside the frontal zone. A geostrophic portion of this flow is, from (6.1a),

$$fv_g = \frac{g}{\rho_o}\int_z^0 \frac{\partial \rho}{\partial x}\,dz \tag{6.3}$$

where the hydrostatic relation $\partial\rho/\partial z = -\rho g$ has been used. The cross-shelf pressure due to cross-shelf slope of sea level does not contribute in the windless case. The third part is driven by the alongshore density gradient induced by the inhomogeneous distribution of alongshore river discharge. The near-bottom velocity of this part can be estimated from a vertical integration of (6.1b):

$$v_{\rho y} = \frac{-g}{r\rho_o}\frac{\partial \bar{\rho}}{\partial y}\frac{h^2}{2}, \qquad (6.4)$$

where $\partial\rho/\partial y$ is assumed constant with depth and is approximately equal to $\partial\bar{\rho}/\partial y$, its vertically averaged value.

To obtain an absolute velocity $v_{\rho x}$ induced by $\partial\rho/\partial x$ we note from a vertical integration of (6.1b) that $v_\rho x(x, y, z = -h) = 0$ when wind is zero; so that by assuming $\partial\rho/\partial x$ is constant over the water depth, (6.3) gives

$$v_{\rho x}(x, y, z) = -\frac{g}{f\rho_o}\frac{\partial \bar{\rho}}{\partial x}(H + z), \qquad (6.5)$$

where $\partial\bar{\rho}/\partial x$ is a vertically averaged value which can be estimated from data.

The total alongshore velocity at stations E and F inside the frontal zone can thus be approximated by

$$v(x_{E,F}, y, z) \approx v_0 + v_{\rho y} + v_{\rho x}. \qquad (6.6)$$

An estimate of $\partial\bar{\rho}/\partial y \approx 10^{-5}$ kg m^{-4} from the seven cruises is rough because of the short period of the experiment. With $H = 8$ m, $r = 3.7 \times 10^{-4}$ m s^{-1}, $v_{\rho y} \approx -8 \times 10^{-3}$ m s^{-1}. For $z = -4$ m and taking $\partial\rho/\partial x = 10^{-4}$ kg m^{-4}, as an average cross-front density gradient from the seven cruises, $v_{\rho x}$ from (6.5) is -4×10^{-2} m s^{-1}. Using (6.6),

$$v(x_{E,F}, y, z) \approx -3.8 \text{ cm s}^{-1}.$$

This compares with the y-intercept values in Table 6 ranging from -1 to -4 cm s^{-1}.

From Table 6 and using $r = 3.7 \times 10^{-4}$ m s^{-1}, we obtain

$$\frac{1}{\rho_o}\frac{\partial p}{\partial y} = \text{PGF}_y \approx g\left[\frac{\partial \xi}{\partial y} + \frac{1}{\rho_o}\frac{\partial \bar{\rho}}{\partial y}\frac{H}{2}\right] \approx 1.0 \times 10^{-6} \text{ m s}^{-2}.$$

Subtracting the contribution from $\partial\bar{\rho}/\partial y$, we obtain an estimate of alongshelf sea level slope of 6×10^{-8} inside the front, or $g\partial\xi/\partial y = 0.6 \times 10^{-6}$ m s^{-2}. Estimating the static wind setup inside the front with $H = 8$ m,

$$g\frac{\partial \xi}{\partial y} \approx \frac{\tau_0{}^y}{H} \approx 2.4 \times 10^{-6} \text{ m s}^{-2}.$$

We now add the Gulf Stream induced pressure gradient force of -2×10^{-6} m s^{-2} and obtain $g\partial\xi/\partial y \approx 0.4 \times 10^{-6}$ m s^{-2}, which compares well with the above estimate of 0.6×10^{-6} m s^{-2} using data from Table 6.

We have examined other data in order to estimate the magnitude of alongshelf sea level slope within the frontal zone. Coastal sea level for Daytona Beach, Florida and Charleston, South Carolina together with wind stress have been used in a simple linear regression model (Schwing et al. 1988). The results, based on data obtained in spring, 1981, show that the zero-stress intercept was positive at Charleston and negative at Daytona Beach. We have interpreted these intercepts as an indication of a net (over the spring season) upward alongshore slope of sea level to the north. The difference in intercepts (0.8 cm)–(−3.1 cm) over a 400 km distance yields a slope of about 1×10^{-7}, or a 4 cm difference in sea level. We interpret this slope as a result of freshwater influxes from estuaries in South Carolina and Georgia and the lack of similar sources off Florida.

To summarize, the coastal front is characterized by a trapped alongshelf pressure gradient manifested by a northward slope of sea level from Florida to South Carolina. This slope, together with the cross-shelf density gradient due to low salinity water within the fronal zone, is consistent with the observed mean flow southwards inside the front. Outside the front, the mean flow is northward and the alongshelf pressure gradient there has the opposite sign. It is probably related to the negative slope of sea level associated with the Gulf Stream.

7. Summary and conclusions

We have used a combination of theory, numerical simulation and field data to gain insight into the dynamics and thermodynamics of momentum and buoyancy fluxes in shallow water coastal frontal zones. In the spring of 1985, the coastal frontal zone contained a trapped alongshore pressure gradient which forced water to flow against the mean wind stress. Sea level sloped upward to the north at 1×10^{-7} inside the frontal zone and changed to a slope of -5×10^{-7} farther offshore outside the frontal zone. The negative slope is presumably due to the northward flowing Gulf Stream since it is unlikely that wind stress conditions in spring could cause a negative slope. The flow field implied by the rapidly changing alongshore pressure gradient across the frontal zone is highly three dimensional, and alongshore and cross-shore velocity gradients are of comparable magnitude.

When alongshore wind stress is positive, low density water is advected offshore, and the isopycnals in the frontal zone become more horizontal. This is reflected by a lowering of potential energy in the frontal zone. When alongshore stress is negative, the slope of the frontal zone steepens as a result of horizontal advection of high density water near surface which induces vertical convection. The potential energy of the system increases.

Acknowledgments. We are indebted to Kathy Bush who calculated heat content and potential energy from the cruise data shown in Fig. 12 and Table 5. We wish to thank Tom Gross and Dave Menzel (SkIO) and Larry Sanford (University of Maryland, Horn Point Laboratory) for their helpful discussions and com-

ments. We also appreciate the work of Susan Salyer and Dee Peterson for preparing the manuscript, and Anna Boyette and Suzanne McIntosh for preparing the illustrations. We gratefully acknowledge the support of the U.S. Department of Energy through Grant DE-FG09-85ER60351.

APPENDIX A

Here we explain how columns 6, 7 and 8 of Table 6 were calculated. We write a simplified alongshore momentum balance as (where now τ_y is the kinematic stress)

$$0 = \frac{1}{h}(\tau_0{}^y - \tau_b{}^y) - \mathrm{PGF}_y \tag{A1}$$

where PGF_y is the total alongshore pressure gradient force. Next we write bottom stress using the linear friction law as

$$\tau_b{}^y = r\bar{v}_b \tag{A2}$$

where r is the linear resistance coefficient and $\bar{v}_b$ is the average alongshore bottom velocity for each wind regime. By substitution

$$0 = \frac{1}{h}(\overline{\tau_0{}^y} - r\bar{v}_b) - \mathrm{PGF}_y \tag{A3}$$

which we rearrange to

$$\bar{v}_b = \frac{1}{r}(\overline{\tau_0{}^y}) - \frac{h}{r}(\mathrm{PGF}_y) \tag{A4}$$

The slope of the line and the y-intercept (yi) from Fig. 12 were used to calculate values of the linear resistance coefficient, the drag coefficient (C_D), and the alongshore pressure gradient force for each current meter (Table 6):

$$r = \frac{1}{(\mathrm{slope})}$$

$$C_D = \frac{r|\bar{v}_b|}{\bar{v}'^2}$$

$$\mathrm{PGF}_y = \frac{(yi)r}{h}$$

See appendix B for discussion of C_D calculations.

APPENDIX B

The simplified momentum balance [Eq. (6.2)] equates τ_y, which is a quadratic function of wind speed, to linearized parameterizations of bottom stress and pressure gradient force. That is, the linear equation form does not parameterize bottom stress as a quadratic function of current speed in the same way that wind stress does. Therefore, we adjusted the linear resistant coefficient, r, as follows:

$$\frac{\tau_b}{\rho} = C_D(\bar{v} + v')^2 \tag{B1}$$

where the bar represents a mean quantity and the prime represents a fluctuation about the mean. Therefore,

$$\frac{\overline{\tau_b}}{\rho} = \overline{C_D(\bar{v} + v')^2} = C_D(\overline{\bar{v}^2 + v'^2})$$

where the long overbars are time averages. Now, define

$$r\bar{v} \equiv \frac{1}{\rho}\bar{\tau}_b = C_D(\overline{\bar{v}^2 + v'^2})$$

Rearranging terms,

$$r\bar{v} = C_D\bar{v}\left(\bar{v} + \frac{\overline{v'^2}}{\bar{v}}\right) \quad \text{or}$$

$$r = C_D\left(\bar{v} + \frac{\overline{v'^2}}{\bar{v}}\right) \tag{B2}$$

Continental shelf currents are characterized by $V'^2 \gg \bar{V}^2$ at tidal and subtidal frequencies. Thus

$$C_D \approx \frac{r|\bar{v}|}{\bar{v}'^2} \tag{B3}$$

The C_D values in Table 6 have been calculated from Eq. (B3).

REFERENCES

Atkinson, L. P., T. N. Lee, J. O. Blanton and W. S. Chandler, 1983: Climatology of the southeastern U.S. continental shelf waters. *J. Geophys. Res.*, **88,** 4705–4718.

Beardsley, R. C., and J. Hart, 1978: A simple theoretical model for the flow of an estuary onto a continental shelf. *J. Geophys. Res.*, **83,** 873–883.

——, and C. D. Winant, 1979: On the mean circulation in the mid-Atlantic Bight. *J. Phys. Oceanogr.*, **9,** 612–619.

Blanton, J. O., 1981: Ocean currents along a nearshore frontal zone on the continental shelf of the southeastern United States. *J. Phys. Oceanogr.*, **11**(12), 1627–1637.

——, 1986: Coastal frontal zones as barriers to offshore fluxes of contaminants. *Rapp. P.-V. Reun. Cons. Int. Explor. Mer,* **186,** 18–30.

——, and L. P. Atkinson, 1983: Transport and fate of river discharge on the continental shelf of the southeastern United States. *J. Geophys. Res.*, **88,** 4730–4738.

Blumberg, A. F., and L. H. Kantha, 1985: Open boundary condition for circulation models. *J. Hydraul. Eng.*, **111,** 237–258.

Griffiths, R. W., and P. F. Linden, 1982: Laboratory experiments on fronts, Part I: Density-driven boundary currents. *Geophys. Astrophys. Fluid Dyn.*, **19,** 159–187.

Hopkins, T. S., and A. Swoboda, 1986: The nearshore circulation off Long Island. *J. Geophys. Res.*, **81,** 5401–5409.

Kantha, L. H., H. J. Herring and G. L. Mellor, 1986: South Atlantic Bight OCS Circulation model, Phase III. Final Report. Prepared for Minerals Management Service, U.S. Dept. Interior (Contract 14-12-0001-29203), 149 pp.

Lee, T. N., V. Kourafalou, J. D. Wang, W. J. Ho, J. O. Blanton, L. P. Atkinson and L. J. Pietrafesa, 1985: Shelf circulation from Cape Canaveral to Cape Fear during winter. *Oceanography of*

the Southeastern U.S. Continental Shelf, L. P. Atkinson, D. W. Menzel and K. Bush, Eds., 33–62.

Mellor, G. L., and T. Yamada, 1982: Development of a turbulent closure model for geophysical fluid problems. *Rev. Geophys. Space Phys.,* **20,** 851–875.

Phillips, O. M., 1966: *The Dynamics of the Upper Ocean.* Cambridge University Press, 261 pp.

Oey, L.-Y., 1986: The formation and maintenance of density fronts on the U.S. southeastern continental shelf during winter. *J. Phys. Oceanogr.,* **16,** 1121–1135.

——, and J. O. Blanton, 1988: Intrusive buoyant plume. Unpublished manuscript.

——, G. L. Mellor and R. I. Hires, 1985: A three-dimensional simulation of the Hudson-Raritan estuary. Part I: Description of the model and model simulations. *J. Phys. Oceanogr.,* **15,** 1676–1692.

——, L. P. Atkinson and J. O. Blanton, 1987: Shoreward intrusion of upper Gulf Stream water onto the U.S. southeastern continental shelf. *J. Phys. Oceanogr.,* **17,** 2318–2333.

Schwing, F. B., L.-Y. Oey and J. O. Blanton, 1985: Frictional response of continental shelf water to local wind forcing. *J. Phys. Oceanogr.,* **15**(12), 1733–1746.

——, ——, and ——, 1988: Evidence for continental shelf waves along the southeastern U.S. during a transitional wind regime. *J. Geophys. Res.,* **93,** 8221–8228.

Scott, J. T., and G. T. Csanady, 1976: Nearshore currents off Long Island. *J. Geophys. Res.,* **81,** 5401–5409.

Simpson, J. H., and D. Bowers, 1981: Models of stratification and frontal movement in shelf seas. *Deep-Sea Res.,* **28A,** 727–738.

——, C. M. Allen and N. C. G. Morris, 1978: Fronts on the continental shelf. *J. Geophys. Res.,* **83,** 4607–4614.

Sturges, W., 1974: Sea level slope along continental boundaries. *J. Geophys. Res.,* **79,** 825–830.

Van Aken, H. M., 1986: The onset of seasonal stratification in shelf seas due to differential advection in the presence of a salinity gradient. *Contin. Shelf Res.,* **5,** 475–485.